Soil creep in a mesotidal salt marsh channel bank: fast, seasonal, and water table mediated

Giulio Mariotti[1,2], William Kearney[3], Sergio Fagherazzi[3]

1 Department of Oceanography and Coastal Sciences, Louisiana State University, 1002-Y Energy, Coast & Environment Building, Baton Rouge, LA 70803

2 Center for Computation and Technology, Louisiana State University, 340 E Parker Blvd, Baton Rouge, LA 70808

3 Department of Earth and Environment, Boston University, 675 Commonwealth Avenue, Boston, MA 02215

Abstract

Muddy banks of marsh channels experience soil creep – a viscous-like slow deformation resulting in a net downslope transport. Here we present the first field evidence of soil creep in a mesotidal salt marsh using both pole displacement and high precision measurements of soil deformation taken with a vibrating-wire extensometer over two years. Soil extended 2-4 mm/m/yr in the high marsh platform and 20-40 mm/m/yr in the low marsh bank. This was equivalent to a soil diffusivity of about 0.2 m^2/yr, which is much higher than the diffusivity on hillslopes and also matches the high value predicted by long-term marsh evolution models. High precision (±0.03 mm) soil deformation measurements shed light on the dynamics of the creep process. First, the low bank compressed and extended by ~5 mm/m every tidal cycle, suggesting that the diurnal changes in water level play a role in the bank movements. Second, net soil extension took place mostly during fall. Net soil extension preceded the period of ice formation, suggesting that freezing and ice rafting are not a leading cause of soil creep. Net soil extension was likely triggered by an increase in water table during fall, which decreased the effective stress

and thus destabilized the bank. This high water table was caused by a combination of an abiotic factor – the increase in atmospheric precipitation – and a biotic factor – the decrease in evapotranspiration triggered by vegetation senescence. This study confirms that creep is a significant process in marsh morphodynamics and that vegetation can reduce mass wasting in marsh channels.

1. Introduction

The presence of blocks observed along the side of marsh channels indicate that marsh banks are subjected to mass wasting. Contrary to sandy banks (Gong et al., 2018), the muddy banks of many salt marshes do not display fast displacement such as planar and rotational failure, but are rather characterized by a slow soil deformation. Individual blocks can be tracked down over many years (Redfield, 1972), indicating that the motion of these blocks is slow compared to the fluvial counterpart. Similarly, the formation and enlargement of extension cracks in banks can be monitored over many years (Deegan et al., 2012). In this context, we use the term soil creep (or bank creep) to include the group of processes resulting in downslope soil flux.

Marsh bank processes are of particular interest because of recent findings related to eutrophication. Nutrient addition has been showed to decrease soil strength (Wigand et al., 2018) and to increase the number of bank cracks and block detachment (Deegan et al., 2012), which is intimately linked to the process of marsh channel bank creep. Yet, the mechanisms by which highly cohesive banks move and their relationship with marsh plants remain unexplored.

Theoretical models for marsh landscape evolution indicate that creep is an important process over decadal to centennial time scales (Kirwan and Murray, 2007; Mariotti, 2018; Mariotti et al.,

2016). Model simulations without creep give rise to channels with steep banks that transition directly into the marsh platform (Mariotti, 2018), a geometry seldom seen in salt marshes. The presence of creep is necessary to reproduce the 5-10 m wide low terrace that is ubiquitous alongside marsh channels with a tidal range greater than about 1 m. Understanding how creep contributes to the formation and evolution of the low marsh terrace is thus especially important in view of the critical ecological role of this area, which provides fish habitat and rapid nutrient removal (Deegan et al., 2012).

Quantifying the rate of bank creep is also important to predict marsh channel widening, a mechanism of marsh loss that has recently accelerated in the North-East coast of the USA (Watson et al., 2017). Furthermore, even in the absence of channel widening, bank creep might still be important for the recycling of both inorganic and organic sediment within salt marshes. Indeed, Mariotti et al. (2016) hypothesized that the sediment in the marsh banks travels in a conveyor-belt: deposits on the low marsh, is transported downslope by creep, is eroded by current flow when it reaches the base of the bank, and eventually re-deposits on the terrace. Quantifying this flux would be important to correctly interpret how much of the sediment accreting on the marsh platform comes from external sources and how much is recycled within the system (Hopkinson et al., 2018; Mariotti and Carr, 2014).

The process of channel bank erosion by creep differs from the process of marsh edge erosion by waves. The latter is characterized by a quick (order of minutes) detachment of large blocks that are subjected to forces oscillating with periods of 2-3 s (the period of sea waves) (Bendoni et al., 2016, 2014; Francalanci et al., 2013). Channel banks are generally sheltered from waves, but might be still subjected to a similar, although slower, instability mechanism. Laboratory experiments revealed that wave-induced block failure takes place when the crack behind the

block is filled with water while the trough of the wave is located just in front of the marsh (Bendoni et al., 2014). A similar force imbalance might be caused by tidal oscillations: during low tide the bank experiences high pore pressure from the saturated soil but does not receive the confining hydrostatic force from the water in the channel. Indeed, laboratory experiments showed that a few tidal cycles were able to detach a block even in the absence of wave action (Francalanci et al., 2013). Noticeably, this mechanism also leads to mass wasting in rivers during the receding phase of a river flood (Deng et al., 2018; Rinaldi and Casagli, 1999), with the differences that rivers experience only a few floods per year, whereas tidal channels generally experience one or two tidal cycles per day.

Marsh evolution models calibrated to fit the bank geometry suggested values of 0.1-0.3 m^2/yr for the creep coefficient (Mariotti, 2018; Mariotti et al., 2016). These values are several orders of magnitude larger than the values found in soil-mantled hillslopes, which generally range between 10^{-5} and 10^{-2} m^2/yr (Pawlik and Šamonil, 2018). The daily tidal cycles might be responsible for such fast rates of soil creep, but no field measurements exist to support this hypothesis.

Another open question is whether soil creep is constant throughout the year or seasonal. Ice rafting, freezing and thawing during winter might play a role in destabilizing the banks at high latitudes (Argow et al., 2011). In addition, vegetation seasonality might affect soil characteristics and therefore mass wasting processes. For example, increased bank stabilization caused by evapotranspiration and reduced pore water pressure was found to be important in rivers only during summer months (Pollen-Bankhead and Simon, 2010). Identifying these effects requires high temporal resolution measurements, which are extremely difficult to obtain over long timescales given the slow rate at which soil creep takes place.

Here we report the first field measurements of channel bank creep using two methods: pole displacement and high-resolution soil deformation through a vibrating-wire extensometer. Pole displacement was measured at different locations in both an undisturbed marsh and a marsh treated with nutrients (Deegan et al., 2012). High resolution measurements were taken at a single location together with water table measurements. Collectively, these measurements are used to shed light on channel bank creep at the hourly, seasonal, and annual time scales.

2. Methods

2.1 Study area

Plum Island Estuary (MA) is a mesotidal system (mean tidal range of 2.9 m) dominated by *Spartina alterniflora* in the low marsh and *Spartina patens* in the high marsh (Fig. 1). The system is representative of the New England region (North-East Coast of the USA), which is characterized by a temperature climate with about 1000 mm of precipitation per year (Table 4), a plant growth season between May to September, and overnight freezes during the winter. Marsh soil is dominated by peat and mud, with a negligible amount of sand except close to the barrier islands (Wilson et al., 2014). High marshes are characterized by a bulk density of ~0.05 kg/m^3 and organic content of ~50%, whereas low marshes are characterized by a bulk density of ~0.1 kg/m^3 and an organic content of ~30% (Wilson et al., 2014).

The study is focused on two marsh sites on which a large scale eutrophication experiment was carried out (Deegan et al., 2012). One site (hereafter referred to as "nutrient enriched") was enriched with nitrogen every incoming tide during each summer from 2004 to 2016, while a nearby site (hereafter referred to as "control") was left untreated (Fig. 1).

111 Here we will refer to bank as a broad term indicating the transitional zone between the
112 channel and the high marsh platform. The terrace (or low terrace) constitutes the lower part of
113 the bank, is located approximately between MSL and MHW, and roughly coincides with the low
114 marsh and with the zone dominated by *S. Altenriflora*. The portion of the high marsh platform
115 close to the terrace (a zone dominated by *S. Patens,* with an elevation close to MHW but with a
116 slight bed slope toward the channel) is referred to as bank platform or simply as platform.

117 2.2 Field measurements with pole displacement

118 Soil deformation was measured at 16 locations: 8 in the control site and 8 in the nutrient
119 enriched site. Soil deformation was calculated by measuring the distances between poles inserted
120 vertically into the ground (Fig. 1D) and left on site for the whole study period (3 years). The
121 distance was measured with a tape placed at the base of the pole. Tape measurements were only
122 taken in the winter, when vegetation was absent, to reduce tape deformation. Measurements were
123 taken on both the high marsh platform and low marsh terrace within the bank of a channel. For
124 the marsh platform the distance was taken from a reference pole (inserted 1 m into the ground) to
125 two measuring poles placed about 0.2 m apart perpendicular to the transect (Fig. 1F). One pole
126 was inserted 0.25 m into the ground, the other was inserted 0.5 m into the ground. Each pole
127 protruded about 0.2 m above the ground. For the low marsh, the distance was measured from the
128 0.5 m pole to a pole placed in the terrace (this pole was inserted to a depth of 0.5 m). The initial
129 distance between each pole was about 2 m. The distance between the poles was measured in
130 December 2015, December 2016, and April 2018, which is considered representative of winter
131 2017 given that plant growth starts in May. Comparisons between the nutrient-enriched and
132 reference sites were performed using the two-sample Kolmogorov-Smirnov goodness-of-fit
133 hypothesis test with the threshold for significance set at 5%.

134 2.3 High-resolution soil deformation

135 A vibrating-wire extensometer (model 4435, Geokon, USA) was deployed in a channel
136 bank in the control site (Fig. 1). The extensometer is composed of four telescopic segments, each
137 one meter long and connected at each end with metal plates 50 cm wide and 30 cm high (Fig. 1).
138 A trench 4 m long, 30 cm deep, and 3 cm wide was dug and the instrument was inserted pushing
139 the five plates into the ground (Fig. 1). The instrument measured the length of each segment
140 every hour, with a resolution of 0.03 mm and an accuracy of 0.1 mm. Because the segments were
141 solidly attached to each other, the length of each segment was affected by the motion of the
142 plates at both ends. The topmost plate was deployed at the transition between marsh platform and
143 bank terrace, so that all segments laid in the terrace area. A 2 cm wide and 50 cm long soil crack
144 was present between the two uppermost plates; no other cracks were detected. Soil temperature
145 was also measured at the uppermost segment. The instrument was deployed on June 21th 2016
146 and the recording stopped on March 6th 2018. A 47 days gap was present between May 18th 2017
147 and July 5th 2017, and the uppermost segment stopped working after October 26th 2017.

148 The bank was photographed hourly with a game camera (A-30, Moultrie, USA) mounted
149 on a fixed post. The bank was surveyed with an RTK-GPS (HiPer Lite+, Topcon, USA).
150 Groundwater level was measured hourly in three wells from the beginning of the deployment
151 until spring 2017 using pressure sensors (Van Essen CTD Diver, USA). The wells were
152 positioned on a transect parallel to the extensometer at a distance of 3 m (Fig. 1). The bed
153 elevation at the well location was 0.5 m above MSL for well 1, 1.1 m above MSL for well 2, and
154 1.2 m above MSL for well 3. Seasonal differences in water table were compared with the two-
155 sample Kolmogorov-Smirnov test. Surface water level was also measured in the middle of the
156 channel (bed elevation -1.3 m with respect to MSL) using a pressure sensor (RBR, Canada),

157 which recorded hourly from October 2015 to December 2016. Water level and air temperature
158 from the NOAA Boston station were used for comparison, given that these data were available
159 for the whole period during which the extensometer was recording.

160 Finally, three datasets collected by the Plum Island Estuary Long Term Ecological
161 Research network were used to complement our measurements. Precipitation was measured
162 every 15 minutes during 2016 and 2017 at a weather station (Marshview Farm**,** 42.756971 N,
163 70.891366 W) located about 4 km northwest of the study site (Giblin, 2018, 2017).
164 Evapotranspiration, calculated based on the latent heat eddy covariance flux (Baldocchi et al.,
165 1988), was measured half-hourly in 2017 on the high marsh platform at a site (42.74244 N,
166 70.83022 W) located about 1 km east of the study site (Giblin and Forbrich, 2018). Aboveground
167 vegetation was measured monthly from 1999 to 2017 in a *Spartina alterniflora* dominated site
168 (Law's Point, 42.731742 N, 70.842472 W) located about 1 km southeast of the study site (Morris
169 and Sundberg, 2018). Plant height was measured non-destructively on the same three control
170 plots and was converted to biomass using allometric relationships (Morris and Sundberg, 2018).

171 **3. Results**

172 3.1 Pole displacement

173 The average precision of the pole displacement method (the average of the difference
174 between two readings taken at the same pole at the same time) was 5 mm. The precision of the
175 collective measurements from each area is set equal to the standard deviation, which includes
176 both the error of the single measurement as well as the actual variability between different
177 locations. This error ranges from about 5 mm for the marsh platform to about 30 mm for the
178 marsh terrace (Table 1). When all measurements from the marsh platform were combined (for
179 both the deep and shallow poles, for both the reference and nutrient-enriched area, and for the 3

time intervals), the average soil extension was 4±5 mm/m/yr (Table 1,S1,S2). No statistical difference between the extension measured with the pole inserted 25 and 50 cm into the ground was found (Table 1). The marsh with nutrients experienced a slightly smaller extension rate than the reference marsh (Table 1), which was however not statistically different. When considering all measurements for the low marsh terrace (including all time intervals for both the reference and nutrient enriched site), the extension was 33±26 mm/m/yr (Table 1,S1,S2). Also in this case, the extension for the nutrient-enriched area was slightly smaller but not statistically different than for the reference area.

3.2 Extensometer

At the yearly time scale the soil extended more in the upper two segments (17±3 mm/m/yr) than in the lower two segments of the extensometer (Fig. 2). One of the lower segments (number 2) had a compression of about 5 mm during the first month, but otherwise the extension was nearly zero in the lower two segments for most of the time. Both lower segments started to extend toward the end of the deployment (Spring 2018), when they extended by about 5 mm each (Fig. 2).

Soil extension showed a clear seasonal trend: in both years nearly 80% of the net soil extension took place in the fall (Fig. 2). This coincided with the period of plant senescence, as indicated by the field photographs as well as by measurement of aboveground biomass in the nearby site (Fig. 3,4A). Field photographs also show that snow and ice were present on the marsh only starting in mid-December (Fig. 3), when air temperature started to drop below freezing (Fig. 2).

Tide-induced fluctuations in soil extension were also detected (Fig. 2,5). These fluctuations were larger in the upper two segments than in the lower two segments. At the upper

segments the soil was about 5 mm more compressed during high tide than during low tide (Fig. 5). Segment 4 displayed a regular pattern of compression during flood and extension during ebb. Segment 3 showed a more complicate pattern: during flood the soil initially compressed and then extended, whereas during ebb the soil first extended and the compressed (Fig. 5).

3.3 Water table

The water table oscillated in response to the tide (Fig. 6), but there was no clear relationship with the spring-neap modulation, i.e., with the range of individual tidal cycles. Despite the large variability, a difference was detected between the summer and fall/winter water table (Fig. 6). Taking as reference well number 2, the water table during the summer 2016 was up to 30 cm below the bed surface, whereas in the fall and winter 2016 only dropped up to 20 cm. Larger drops in water level started to occur in spring 2017, after which the measurements ended. The 5^{th} percentile of the water table was 0.23 m below the bed surface in summer, 0.18 m in fall, and 0.16 m in winter. The Kolmogorov-Smirnov test indicated that the fall and winter water levels did not different significantly from each other, whereas the water table was significantly different between fall/winter and summer.

Although net soil extension took place throughout the fall, in several occasions this extension was concentrated in a very short time period (Fig. 6). In particular, two episodes of rapid soil extension were detected during fall 2016 (day 122 and day 147). These two episodes had an anomalous water table behavior, i.e., the water table dropped about 0.1 m less than expected from the previous tidal cycles (Fig. 7C-E). These two episodes also coincided with intense atmospheric precipitation (about 80 mm of rain in a day) (Fig 6F).

4. Discussion

225 4.1 Soil extension at the yearly time scale

226 The large number of measurements with the pole displacement method allowed to obtain
227 two robust results. First, the terrace extended much more than the platform. Second, because the
228 displacement measured at poles inserted at different depths (0.25 and 0.5 m) was nearly
229 identical, we infer that creep took place over a depth greater than 0.5 m. These measurements
230 also showed that the soil in the nutrient enriched site extended less than in the reference site, but
231 the difference was not statistically significant. This result disagrees with recent finding of
232 reduced soil strength in the nutrient enriched site compared to the reference site (Wigand et al.,
233 2018). One possible interpretation is that nutrient enrichment had an effect smaller than the
234 natural variability in bank creep. The other possible explanation is that the nutrient enriched
235 marsh relaxed to the perturbation caused by the nutrient addition – which started in 2004 – and
236 adjusted its geometry to create a gentler slope and a smaller creep. In other words, most of the
237 nutrient effect on bank creep took already place, and the bank is now creeping at a slower rate
238 despite the soil being weaker.

239 The extension measured with the poles located in the terrace overlaps with the extension
240 of the two upper segments of the extensometer (Fig. 1). The two measurements gave remarkably
241 similar values considering the errors and the spatial variability of the processes: 17±3 mm/yr for
242 the extensometer and 33±26 mm/m/yr for the pole displacements. The large variability of the
243 latter is not given by the precision of the measurement, which is estimated to be 5 mm, but likely
244 reflects the heterogeneities of the marsh banks, for example irregularities in the geometry and
245 heterogeneities in plant and peat properties.

246 The extension measurements did not track the absolute value of soil displacement, i.e.,
247 the velocity at which the soil moves horizontally, U, but rather the difference in soil

displacement between plates. As such, the total soil displacement at each point should be calculated by summing the relative displacements of the plates above. Taking the position of plate 5 (the top plate) as reference, plate 1 (the lower part of the bank) moved at about 48 mm/yr compared to the 20 mm/yr of plate 4. In other words, that the lack of extensions in the two lowermost segments does not indicate absence of soil motion, but instead suggests that the creep flux is spatially uniform in the lower part of the bank.

The lack of extension in the lower segments is consistent with the geometry of the bank: the gradient in bed slope, i.e., the curvature, is large in the upper segments but is nearly zero in the lower segments (Table 2). The soil extension and the gradient in bed slope can be used to calculate the (linear) creep coefficient μ using the formula:

$$\frac{\mathrm{d}F}{\mathrm{d}x} = \frac{\mathrm{d}(hU)}{\mathrm{d}x} = \mu \frac{\mathrm{d}S}{\mathrm{d}x} \qquad (1)$$

where F is the volumetric creep flux per unit of width, h is the depth of the creeping layer (i.e., the depth below which creep is no more present), S is the bed slope along the transect, and x is the coordinate along the transect. The depth of the creeping layer is assumed equal to 1 m, which is larger than the lower limit estimated by the high marsh pole displacement (0.5 m) and less than the thickness of the peat layer, which is about 2 m (Hein et al., 2012; Wilson et al., 2014). For each segment, the gradients in slope can be calculated using the slope of the two adjacent segments (Table 2). The resulting coefficient for the four segments ranges from 0.1 to 0.3 m^2/yr (Table 2). Assuming that the curvature where the low marsh pole displacement was measured is the same as the curvature at segment 3 and 4 of the extensometer, the resulting creep coefficient from the pole displacement is 0.18 m^2/yr.

The estimate of the soil diffusivity is affected by the error in measuring soil displacement, the error in measuring the marsh slope, and the error in assuming the depth of the creeping layer, which overall can give an uncertainty of at least a factor of two. It is however remarkable that the estimated coefficient is of the same order of magnitude of the value estimated from a mathematical model that was calibrated to match the observed marsh bank curvature (Mariotti et al., 2016), and that this coefficient is four orders of magnitude larger than typical values for soil-mantled hillslopes (Pawlik and Šamonil, 2018).

4.2 Intra-tidal fluctuations

The high precision measurements reveal that the soil oscillates back and forth with each tidal cycle (Fig. 5). Because the length of each segment depends on the motion of both plates at its ends, the pattern of extension and compression are related in a non-trivial way to the tidal oscillations. Specifically, the measurements at segment 3 suggest the presence of a compression-extension wave that propagate up-bank during the rising limb of the tide and down-bank during the falling limb.

We suggest that the oscillations in the water level cause a fatigue like behavior. Every time the water level drops, the bank remains nearly saturated (because of the low permeability) but loses the confining hydrostatic pressure from the channel – similar to the drawdown dynamics during the receding phase of a river flood (Deng et al., 2018; Luppi et al., 2009; Rinaldi and Casagli, 1999) – which causes the soil to extends by a small amount. For most tidal cycles the high tide compresses the soil back to the original position. In some instance, however, soil extends more than usual during low tide, and this excess is not compensated by the following compression at high tide. Over many cycles this process leads to the large extension measured in the upper part of the terrace.

Noticeably, the high water table in the bank during low tide is also the driving mechanism for mass wasting in sandy and unvegetated tidal creeks (Gong et al., 2018). Indeed, a modeling work showed that tidal creek bank failure is strongly mediated by the water table (Gong et al., 2018), and resembles the river dynamics during the receding phase of a river flood, during which the water table in the bank is high and the water level in the channel is low (Luppi et al., 2009). We thus speculate that water table mediates mass wasting in both sandy and muddy marsh banks, but results in different outcomes depending on soil properties: in weakly-cohesive banks it triggers failure, i.e., displacement of large blocks by a few meters in a time scale from seconds to hours, whereas in muddy (cohesive) marsh banks it promotes creep, which proceeds at much slower rates than failure.

The absence of a relationship between soil deformation and spring-neap tidal modulation suggests that the creep process is largely independent of tidal range. Indeed, the maximum water table gradients is determined by the bank geometry, specifically by the height of the bank with respect to the study area, and not by the amount of water above the marsh platform. As such we speculate that this process occurs everywhere the low tide is low enough to expose the base of the channel bank, which is generally the case in mesotidal and macrotidal settings. In accordance with this idea, a storm surge that occurred on January 4th 2018 (high water 2.8 above MSL and 1.2 m above the high marsh platform) did not record any detectable signal at the extensometer (Fig. 2F). This observation also confirms that even extreme wave events associated with storm surges do not affect channel bank dynamics, at least in channels with widths smaller than a few tens of meters.

4.3 Seasonal dynamics

During both years, net soil extension was concentrated in the fall. In both years the extension preceded the period of snowfall and soil freeze (Fig. 2,3), suggesting that ice rafting (Argow et al., 2011) is not a leading cause of soil creep in channel banks. We however acknowledge that rafting might create localized and high-intensity bank movements that were not captured by the high-precision measurements, which were only collected at one location. Is therefore possible that rafting might constitute an additional process that would add to the creep estimated from the extensometer measurements.

One mechanism that might explain the faster creep in the fall is the relative increase in water table with respect to the summer period (Fig. 6D). A low water table in the bank during the summer increases the effective soil stress and thus stabilize the bank. A higher water table in the fall could reduce the effective stress, increase the force imbalance that establishes at low tide, and thus destabilize the bank. Indeed, this force imbalance is the same mechanism that drives failure of weakly cohesive banks in both rivers and salt marsh channels (Deng et al., 2018; Gong et al., 2018; Luppi et al., 2009).

The observed increase in water table during fall is likely related to atmospheric precipitation, which was three times larger during fall than in summer. This atmospheric control is particularly evident during two events with about 80 mm of precipitation (Fig. 6F), which are correlated with an anomalously high water table and anomalously large net soil extension (Fig. 6). On the other hand, not all precipitation events triggered extension events (Fig. 6), and a much gradual extension took place throughout fall – especially in 2017 – even in the absence of intense precipitation events. Thus, despite intense precipitation events might cause micro-failure of the bank, a more uniform (i.e., not event-based) process must be present throughout the fall.

335 The other mechanism that could have contributed to the high water table during fall is a
336 reduction in evapotranspiration, which is clearly detected from the eddy flux measurements (Fig.
337 4B). This is likely related to the reduction in evaporation caused by the drastic drop in air
338 temperature. In addition, plant senescence might have played an important role. *Spartina*
339 *alterniflora* in the low marsh terrace is indeed known to actively change the soil conditions to
340 keep the rhizosphere aerated (Bertness, 1991). This plant transpiration – only present during
341 summer – can lower the marsh water table by a few centimeters within hours (Dacey and Howes,
342 1984). Thus, as for the riverine case (Pollen-Bankhead and Simon, 2010), the absence of plant
343 activity in the fall could have caused a relative increase in water table and destabilized the bank.

344 Marsh plants could have also destabilized the bank by changing the soil geotechnical
345 properties, for example by reducing root strength and soil cohesion. A study in salt marshes
346 within Terrebonne and Barataria Bay (Louisiana, USA) showed that the tensile root resistance
347 of *Spartina alterniflora* (the same species present on the banks in our study site) was smaller in
348 winter and spring than in summer (Bouanchaud III, 2013). Despite the different climate, the
349 study from Louisiana (a subtropical region) might suggests the presence of a similar seasonal
350 trend in the marshes of Plum Island Estuary. We argue however that this could not be the only
351 factor explaining the patterns in soil extension at our site. Indeed, the increase in net extension
352 started at the very beginning of each fall, whereas an alteration of the soil structure would have
353 likely lagged after the beginning of plant senescence. On the other hand, evapotranspiration
354 would have responded almost immediately to seasonal changes and thus seems a more likely
355 candidate to explain the observed trends. Further field investigations are required to assess
356 whether seasonal changes in soil properties are present in temperate salt marshes as those of
357 Plum Island Estuary.

An open question is why the net extension observed during winter was greater than summer but smaller than fall. The water table in winter was as high as in fall, suggesting that other mechanisms are involved. One possible explanation is that in winter the soil does not have the destabilizing forces associated with the weight of aboveground component of the plants (Fig. 3). The dead plants hanging from the marsh terrace could also act as an anchor during the falling tide and exert an additional destabilizing force on the bank, which would be present during fall but not during winter. Another explanation is that soil geotechnical properties gradually change from fall to winter. For example, freezing might stiffen the soil and decrease its ability to deform. This is confirmed by the reduction in the amplitude of tide-induced soil fluctuation when the soil temperature drops below -1 °C (Fig. 8). A reduction in microbial activity might have also caused some seasonal changes in soil properties. For example, sulfate reduction has been shown to remain high from summer throughout the fall, but to drastically decrease in winter (Howarth and Teal, 1979). Whether this change could have consequences on soil shear strength, for example through changes in pH (Ghobadi et al., 2014), needs to be tested with further field measurements over different seasons.

We now discuss whether these observations could apply to other salt marshes outside Plum Island Estuary. The two years considered were characterized by temperature and precipitation in line with the long term trends (Table S4), suggesting that the measurements are representative of average conditions. Furthermore, the soil extension was remarkably similar over the two years (despite the presence of a major storm surge), suggesting that bank creep is regular over multiple years. It is thus plausible to assume that a water table and bank dynamics similar to the one here observed might be present in marshes with similar climates, such as those

380 in the New England region. In these marshes we expect that mass wasting – either by creep in
381 cohesive banks or by failure in weakly-cohesive banks – will occur during the fall.

382 4.4 Consequences for salt marsh ecogeomorphology and stratigraphy

383 Our measurements highlight that the marshes of Plum Island Estuary experience mass
384 wasting by soil creep. This modality of sediment transport is different from surface erosion by
385 current flow (Gong et al., 2018), even though surface erosion can erode the base of the bank,
386 increase bank slope, and in thus increase bank creep (Mariotti et al., 2016). Because this type of
387 mass wasting might be present in other highly cohesive marshes, this result confirms the
388 importance of including a soil diffusion mechanism to parameterize bank processes in models for
389 salt marsh evolution (Kirwan and Murray, 2007; Mariotti, 2018).

390 Our results also suggest that vegetation stabilizes marsh channel banks by reducing the
391 elevation of the water table through evapotranspiration. Climatic and meteorological processes
392 that change plant evapotranspiration, such as droughts and global warming, could thus have an
393 effect on bank stability. In addition, removal of aboveground plants by grazing (Bertness et al.,
394 2014) could cause a sudden bank destabilization and channel widening even in the absence of
395 root decay or changes in belowground soil properties.

396 Bank creep is able to transport sediment from the marsh to the channel. To put this
397 sediment flux into perspective, we evaluate how the lateral transport by bank creep compares to
398 the vertical accretion on the marsh platform. We calculate the volumetric bank sediment flux as
399 $Uh2L$, where L is the total length of the channel network. The vertical accretion is calculated
400 assuming that the marsh accretes at the same rate of relative sea level rise, R. As such, the ratio
401 between lateral flux and vertical flux is $\frac{2UhL}{RA}$, where A is the total marsh area. For the marshes of

Plum Island Estuary, the ratio L/A is equal to about 0.02 m^{-1} (Wilson et al., 2014). Taking U equal to 48 mm/yr, h equal to 1 m, and R equal to 2.7 mm/yr (Wilson et al., 2014), the ratio between bank flux and vertical accretion flux is 0.71. Despite bank creep might be variable in space, this result suggests that the amount of sediment transported by bank creep is the same order of magnitude of the amount of sediment that accumulates over the whole marsh platform. This result thus supports the hypothesis that a large fraction of the organic and inorganic sediment that deposits on the marsh is recycled within the salt marsh (Hopkinson et al., 2018; Mariotti and Carr, 2014).

The presence of channel bank creep could also modify marsh stratigraphy, similarly to the way that soil creep in hillslopes modifies the dip of beds along roadcuts (Stearn, 1935). Because of the horizontal displacement caused by creep, sediment that is initially deposited at high-marsh elevation (for example at the position of plate 5, Fig.1) is slowly transported toward the channel and toward lower elevations (for example at plate 3). Here the sediment will get buried with time by newer sediment. This new sediment would incorporate indicators of the current elevation, that is, low-marsh indicators. As a result, even at steady state (i.e., without changes in sea level or sediment supply), high marsh soil (i.e., soil with roots of high marsh plants such as *Spartina patens*) might be found underneath soil that incorporates low marsh indicators. This mechanism can have important consequence when the vertical stratigraphy of marsh banks is used to reconstruct past sea level (Donnelly and Bertness, 2001). For example, an inverted sequence of high marsh soil underneath a low marsh soil has been found in a New England marsh and it has been interpreted as a sign of sea level acceleration (Donnelly and Bertness, 2001). The presence of creep suggests that this inverted sequence might be found on channel banks of salt marshes even without an accelerating sea level rise. Further investigation

should be directed to evaluate how bank creep affects stratigraphy and what corrections should be considered while interpreting cores taken from channel banks.

To conclude, we emphasize that the most unconstrained aspect of the bank creep mechanism is the depth of the creep layer, which here was assumed to be equal to 1 m. An extensive literature on hillslope creep (Pawlik and Šamonil, 2018) suggests that this depth likely depends on soil properties (grain size, clay content, bulk density, organic matter content), vegetation properties, biological activity, climate, and stratigraphy. Our measurements indicate that this depth is likely larger than 0.5 m, but the upper limit is largely unconstrained, and is possible that creep might also occur in the estuarine mud layer underneath the peat (i.e., at depths larger than 2 m). The vertical profile of creep velocity should be further investigated in the field, for example installing multiple extensometers at different depths over the same transect.

5. Conclusions

We report the first measurements of bank creep in the marshes of Plum Island Estuary (MA, USA). Two independent methods both found a soil diffusivity of 0.1-0.3 m^2/yr, which matches the predictions of previous marsh evolution models and confirms that this diffusivity is several orders of magnitude larger than on soil-mantled hillslopes. This study thus confirms that soil creep is significant processes at least in the study area and possibly in other marshes with similar characteristics: temperate climate, mesotidal regime, and highly cohesive sediments. We conclude that bank creep is important to 1) simulate the geometry and morphodynamics of channels and low marsh terrace, 2) calculate sediment fluxes to and from the marsh, and 3) interpret the stratigraphy of channel banks.

High precision measurements indicate that bank creep in Plum Island Estuary takes place mostly during fall. This pattern is likely due to an increase in water table, which in turn is caused

by an increase in atmospheric precipitation and a decrease in evapotranspiration. Because plant transpiration can actively lower the water table, our measurements are an indirect proof that marsh plants reduce mass wasting in marsh channels, and that climate change could potentially alter the dynamics of marsh banks.

Acknowledgments

SF and WK were supported by the National Science Foundation (awards OCE1354251, OCE1354494, OCE1637630 and DEB1237733). Data are publicly available through the Long Term Ecological Research (LTER) Network Data Portal at http://portal.lternet.edu.

References

Argow, B.A., Hughes, Z.J., FitzGerald, D.M., 2011. Ice raft formation, sediment load, and theoretical potential for ice-rafted sediment influx on northern coastal wetlands. Cont. Shelf Res. 31, 1294–1305. https://doi.org/10.1016/j.csr.2011.05.004

Baldocchi, D.D., Hincks, B.B., Meyers, T.P., 1988. Measuring Biosphere-Atmosphere Exchanges of Biologically Related Gases with Micrometeorological Methods. Ecology 69, 1331–1340. https://doi.org/10.2307/1941631

Bendoni, M., Francalanci, S., Cappietti, L., Solari, L., 2014. On salt marshes retreat: Experiments and modeling toppling failures induced by wind waves. J. Geophys. Res. Earth Surf. 119, 603–620. https://doi.org/10.1002/2013JF002967

468 Bendoni, M., Mel, R., Solari, L., Lanzoni, S., Francalanci, S., Oumeraci, H., 2016. Insights into
469 lateral marsh retreat mechanism through localized field measurements. Water Resour.
470 Res. 52, 1446–1464. https://doi.org/10.1002/2015WR017966

471 Bertness, M.D., 1991. Zonation of Spartina Patens and Spartina Alterniflora in New England Salt
472 Marsh. Ecology 72, 138–148. https://doi.org/10.2307/1938909

473 Bertness, M.D., Brisson, C.P., Bevil, M.C., Crotty, S.M., 2014. Herbivory Drives the Spread of
474 Salt Marsh Die-Off. PLOS ONE 9, e92916. https://doi.org/10.1371/journal.pone.0092916

475 Bouanchaud III, J.M., 2013. The uplift resistance of Spartina Alterniflora in a Louisiana salt
476 marsh. LSU Masters Theses 3044.

477 Dacey, J.W., Howes, B.L., 1984. Water uptake by roots controls water table movement and
478 sediment oxidation in short spartina marsh. Science 224, 487–489.
479 https://doi.org/10.1126/science.224.4648.487

480 Deegan, L.A., Johnson, D.S., Warren, R.S., Peterson, B.J., Fleeger, J.W., Fagherazzi, S.,
481 Wollheim, W.M., 2012. Coastal eutrophication as a driver of salt marsh loss. Nature 490,
482 388–392. https://doi.org/10.1038/nature11533

483 Deng, S., Xia, J., Zhou, M., Li, J., Zhu, Y., 2018. Coupled modeling of bank retreat processes in
484 the Upper Jingjiang Reach, China. Earth Surf. Process. Landf. 43, 2863–2875.
485 https://doi.org/10.1002/esp.4439

486 Donnelly, J.P., Bertness, M.D., 2001. Rapid shoreward encroachment of salt marsh cordgrass in
487 response to accelerated sea-level rise. Proc. Natl. Acad. Sci. 98, 14218–14223.
488 https://doi.org/10.1073/pnas.251209298

Francalanci, S., Bendoni, M., Rinaldi, M., Solari, L., 2013. Ecomorphodynamic evolution of salt marshes: Experimental observations of bank retreat processes. Geomorphology 195, 53–65. https://doi.org/10.1016/j.geomorph.2013.04.026

Ghobadi, M.H., Abdilor, Y., Babazadeh, R., 2014. Stabilization of clay soils using lime and effect of pH variations on shear strength parameters. Bull. Eng. Geol. Environ. 73, 611–619. https://doi.org/10.1007/s10064-013-0563-7

Giblin, A., 2018. Year 2017, meteorological data, 15 minute intervals, from the PIE LTER Marshview Farm weather station located in Newbury, MA. Environmental Data Initiative. Plum Isl. Ecosyst. LTER Long Term Ecol. Res. Netw. https://doi.org/10.6073/pasta/80e0962b53d2549002fcc53eaf7394c6. Dataset accessed 8/16/2018.

Giblin, A., 2017. Year 2016, meteorological data, 15 minute intervals, from the PIE LTER Marshview Farm weather station located in Newbury, MA. Environmental Data Initiative. Plum Isl. Ecosyst. LTER Long Term Ecol. Res. Netw. https://doi.org/10.6073/pasta/d5bfbfc6de185cff9b7302884c78e0fe. Dataset accessed 8/16/2018

Giblin, A., Forbrich, I., 2018. PIE LTER Eddy flux measurements during 2017 from second high marsh site (Spartina patens/short Spartina alterniflora) Tall Tower off Nelson Island Creek, Rowley, Massachusetts. Environmental Data Initiative. Plum Isl. Ecosyst. LTER Long Term Ecol. Res. Netw. https://doi.org/10.6073/pasta/b718d36c4c0c3c6ef1eea5dbbdc77074. Dataset accessed 8/16/2018.

511 Gong, Z., Zhao, K., Zhang, C., Dai, W., Coco, G., Zhou, Z., 2018. The role of bank collapse on
512 tidal creek ontogeny: A novel process-based model for bank retreat. Geomorphology 311,
513 13–26. https://doi.org/10.1016/j.geomorph.2018.03.016

514 Hein, C.J., FitzGerald, D.M., Carruthers, E.A., Stone, B.D., Barnhardt, W.A., Gontz, A.M.,
515 2012. Refining the model of barrier island formation along a paraglacial coast in the Gulf
516 of Maine. Mar. Geol. 307–310, 40–57. https://doi.org/10.1016/j.margeo.2012.03.001

517 Hopkinson, C.S., Morris, J.T., Fagherazzi, S., Wollheim, W.M., Raymond, P.A., 2018. Lateral
518 Marsh Edge Erosion as a Source of Sediments for Vertical Marsh Accretion. J. Geophys.
519 Res. Biogeosciences 123, 2444–2465. https://doi.org/10.1029/2017JG004358

520 Howarth, R.W., Teal, J.M., 1979. Sulfate reduction in a New England salt marsh1. Limnol.
521 Oceanogr. 24, 999–1013. https://doi.org/10.4319/lo.1979.24.6.0999

522 Kirwan, M.L., Murray, A.B., 2007. A coupled geomorphic and ecological model of tidal marsh
523 evolution. Proc. Natl. Acad. Sci. 104, 6118–6122.
524 https://doi.org/10.1073/pnas.0700958104

525 Luppi, L., Rinaldi, M., Teruggi, L.B., Darby, S.E., Nardi, L., 2009. Monitoring and numerical
526 modelling of riverbank erosion processes: a case study along the Cecina River (central
527 Italy). Earth Surf. Process. Landf. 34, 530–546. https://doi.org/10.1002/esp.1754

528 Mariotti, G., 2018. Marsh channel morphological response to sea level rise and sediment supply.
529 Estuar. Coast. Shelf Sci. https://doi.org/10.1016/j.ecss.2018.05.016

530 Mariotti, G., Carr, J., 2014. Dual role of salt marsh retreat: Long-term loss and short-term
531 resilience. Water Resour. Res. 50, 2963–2974. https://doi.org/10.1002/2013WR014676

Mariotti, G., Kearney, W., Fagherazzi, S., 2016. Soil creep in salt marshes. Geology 44, 459–462.

Morris, J.T., Sundberg, K., 2018. Morris J., K. Sundberg. 2018. Aboveground biomass data from control sites in a Spartina alterniflora-dominated salt marsh at Law's Point, Rowley River, Plum Island Ecosystem LTER, MA.. Environmental Data Initiative. Plum Isl. Ecosyst. LTER Long Term Ecol. Res. Netw. https://doi.org/10.6073/pasta/f039a76cf0dff2f8033ce930de9b8c3d. Dataset accessed 8/16/2018.

Pawlik, Ł., Šamonil, P., 2018. Soil creep: The driving factors, evidence and significance for biogeomorphic and pedogenic domains and systems – A critical literature review. Earth-Sci. Rev. 178, 257–278. https://doi.org/10.1016/j.earscirev.2018.01.008

Pollen-Bankhead, N., Simon, A., 2010. Hydrologic and hydraulic effects of riparian root networks on streambank stability: Is mechanical root-reinforcement the whole story? Geomorphology, Geomorphology and Vegetation: Interactions, Dependencies, and Feedback Loops 116, 353–362. https://doi.org/10.1016/j.geomorph.2009.11.013

Redfield, A.C., 1972. Development of a New England Salt Marsh. Ecol. Monogr. 42, 201–237. https://doi.org/10.2307/1942263

Rinaldi, M., Casagli, N., 1999. Stability of streambanks formed in partially saturated soils and effects of negative pore water pressures: the Sieve River (Italy). Geomorphology 26, 253–277. https://doi.org/10.1016/S0169-555X(98)00069-5

Stearn, N.H., 1935. Structure and creep. J Geol 43, 323–327.

553 Watson, E.B., Wigand, C., Davey, E.W., Andrews, H.M., Bishop, J., Raposa, K.B., 2017.
554 Wetland Loss Patterns and Inundation-Productivity Relationships Prognosticate
555 Widespread Salt Marsh Loss for Southern New England. Estuaries Coasts 40, 662–681.
556 https://doi.org/10.1007/s12237-016-0069-1

557 Wigand, C., Watson, E.B., Martin, R., Johnson, D.S., Warren, R.S., Hanson, A., Davey, E.,
558 Johnson, R., Deegan, L., 2018. Discontinuities in soil strength contribute to
559 destabilization of nutrient-enriched creeks. Ecosphere 9, e02329.
560 https://doi.org/10.1002/ecs2.2329

561 Wilson, C.A., Hughes, Z.J., FitzGerald, D.M., Hopkinson, C., Valentine, V., Kolker, A.S., 2014.
562 Saltmarsh Pool and Tidal Creek Morphodynamics: Dynamic Equilibrium of Northern
563 Latitude Saltmarshes? Geomorphology. https://doi.org/10.1016/j.geomorph.2014.01.002

564

565 **List of figures**

566 Figure 1. A,B,) Geographical location of Plum Island Estuary. C) Satellite image of the marsh in
567 Plum Island Estuary (MA). The squares show the two study sites. The star indicates the site
568 where aboveground vegetation biomass was measured. The location of the extensometer is
569 42.737737° N, 70.848920° W. Image from GoogleEarth, Landsat, acquired in 2017. D) Scheme
570 of the pole displacement measurements. E) Detail of the channel in which the extensometer
571 (segment) and the wells (dots) were installed. The position of plate 1 of the extensometer is
572 42.737745°N and 70.848909°, The position of plate 5 of the extensometer is 42.737718° N and
573 70.848908°W, the position of well 1 42.737736° N and 70.848958°W, the position of well 2 is
574 42.737718°N and 70.848957°W, the position of well 3 is 42.737682°N, 70.848956°W. F)

Photograph of the channel, showing the transition from low to high marsh and the presence of bank slumping. The head of the channel is toward the bottom right. Arrows indicate the position of the three upper plates of the extensometer. The distance between plates (2m) can be used for scale. G) Photograph of the extensometer deployed in the bank. The distance between plates (2 m) and the width of the plates (0.5 m) can be used for scale. H) Measured elevation profile showing the position of the extensometer and the position of the water level sensors in the bank and in the channel bed.

Figure 2. Multi-year trends in soil deformation. A,B,C,D) Soil extension at the four segments. The initial length is set equal to zero for all segments. Segment numbering starts from the bottom of the bank (Fig. 1F). E) Air temperature measured at the NOAA Boston station, soil temperature measured 15 cm below the ground surface at segment 4. The horizontal line indicates the freezing temperature for water with a salinity of 20 PSU (-1 °C). Day zero in the time series corresponds to June 21th 2016. F) Water level measure at the NOAA Boston station. Vertical dashed lines indicate seasons.

Figure 3. Photographs of vegetation taken with a camera mounted on a post positioned on the opposite bank. The platform on which the data logger is located is 1.2 m tall. All photographs are taken at 12 pm. The three arrows in the bottom right panel indicate the position of the three upper plates.

596 Figure 4. A) Aboveground biomass measured in a *Spartina alterniflora* dominated site located
597 about 1 km from the study site (Fig. 1A). The dataset was collected by the PIE-LTER from 1999
598 to 2017 every month from approximately May to approximately October. The data for 2016 and
599 2017, during which the measurements in this study were collected, are shown by the colored
600 dots. B) Evapotranspiration for year 2017, measured by the PIE-LTER using an eddy flux tower
601 located on the high marsh platform ~1 km east of the study site. Blue dots indicate half-hourly
602 measurements, red dots indicate monthly means.

603

604 Figure 5. Details of soil deformation during two representative tidal cycles (see Fig. 2 for
605 reference). A,B) Soil extension in the upper two segments. C) Water level measured in the
606 channel. D) Cartoon explaining the relationship between plate motion and segments
607 extension/compression during different phases, which are indicated with roman numbers.

608

609 Figure 6. Soil deformation trends over multiple seasons (starting from June 21th 2016, as the time
610 series in Figure 2 but ending on April 1st 2017). A,B) Extension of the upper two segments. C)
611 Water level in Boston referred to mean sea level. Spring-neap variations can be clearly detected.
612 D) Water table measured in well 2 (Fig. 1) and referred to the local bed elevation. E) Rate of
613 water table drop in well 2. F) Cumulative precipitation measured ~4 km away from the study
614 sites by the PIE LTER. The vertical arrows indicate two episodic extension events overlapping
615 with two periods of intense precipitation.

616

617 Figure 7. Details of two episodic extension events (see Fig. 6). A,B) Length of the upper two
618 segments. C,D,E) Water table measured at three different wells on the bank and referred to
619 mean sea level (Fig. 1). The gray shadings indicate the episodic extension events. Arrows point
620 to the anomalously high water table.

621

622 Figure 8. Three examples of periods when the fluctuations in soil extension were smaller than
623 average (see Fig. 6 for reference). A,B) Length of the upper two segments. C) Soil temperature
624 measured 15 cm below the ground surface at segment 4. The horizontal line indicates -1 °C, the
625 freezing temperature of sea water. The gray shadings indicate periods with smaller soil
626 oscillations when soil temperature was below -1 °C.

627

628

629

Table 1

Table 1. Rates of soil extension [mm/m/yr] measured using pole displacement. Both mean and standard deviation is reported. The number in parenthesis indicates the number of locations from which measurements were available for that time interval (see Table S1 and S2). Because the winter 2017 measurements were taken on April 2018, the 2016-2017 interval is normalized by 1.3 years and the 2015-2017 interval is normalized by 2.3 years. The average for each location is calculated by considering all the data from the 3 time intervals (2015-2016, 2017-2016, 2017-2015).

	Reference marsh			Nutrient-enriched marsh		
	High marsh (0.5 m pole)	High marsh (0.25 m pole)	Low marsh (0.5 m pole)	High marsh (0.5 m pole)	High marsh (0.25 m pole)	Low marsh (0.5 m pole)
2015-2016	5±6 (*n*=8)	7±7 (*n*=7)	30.0±23 (*n* =8)	-3±1 (*n*=3)	0±4 (*n*=3)	13±7 (*n* =3)
2016-2017	4±4 (*n*=5)	4±4 (*n*=5)	57±30 (*n* =3)	6±5 (*n*=3)	6±5 (*n*=3)	12 (*n* =1)
2015-2017	4±3 (*n*=5)	5±5 (*n*=5)	54 ±31 (*n* =3)	2±3 (*n*=7)	2±1 (*n*=6)	39±28 (*n* =4)
Average	4±4 (*n*=18)	5±5 (*n*=17)	41±27 (*n*=14)	2±5 (*n*=13)	2±4 (*n*=12)	26±23 (*n*=8)

Figure 1

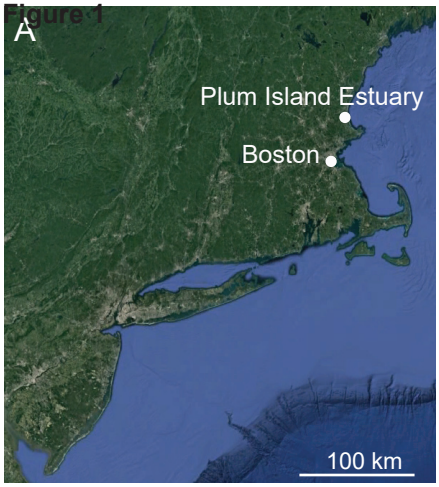
A
Plum Island Estuary
Boston
100 km

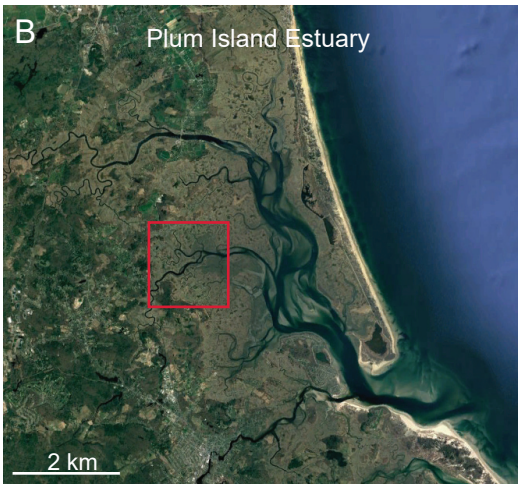
B
Plum Island Estuary
2 km

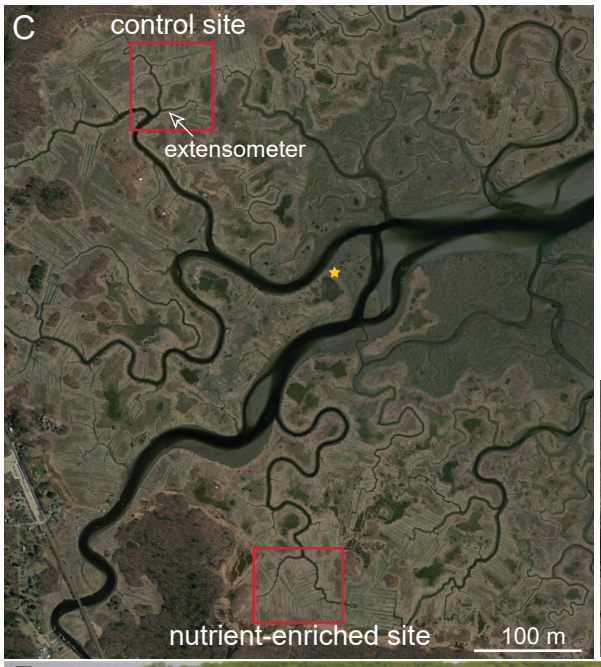
C
control site
extensometer
nutrient-enriched site
100 m

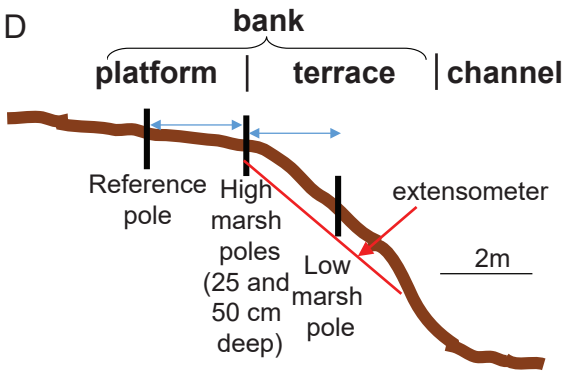
D
bank
platform
terrace
channel
Reference pole
High marsh poles (25 and 50 cm deep)
Low marsh pole
extensometer
2m

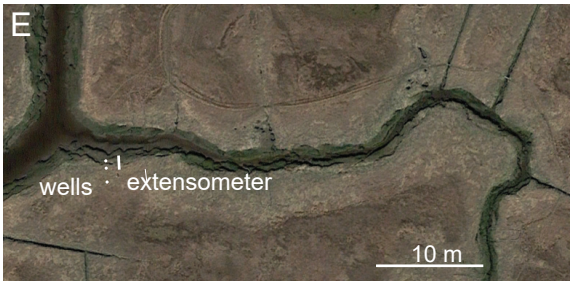
E
wells
extensometer
10 m


F
plate 5
plate 4
plate 3
terrace
platform

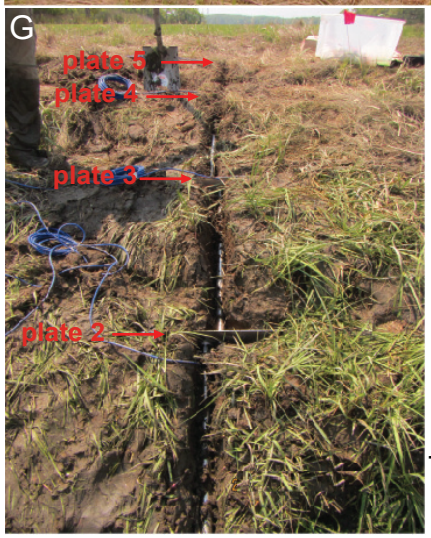
G
plate 5
plate 4
plate 3
plate 2

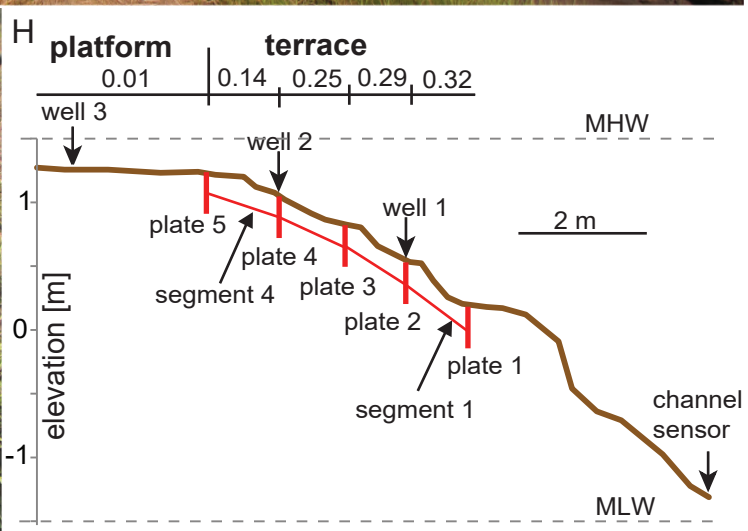
H
platform
terrace
0.01
0.14
0.25
0.29
0.32
well 3
well 2
well 1
MHW
MLW
plate 5
plate 4
plate 3
plate 2
plate 1
segment 4
segment 1
channel sensor
2 m
elevation [m]
1
0
-1

Figure 2

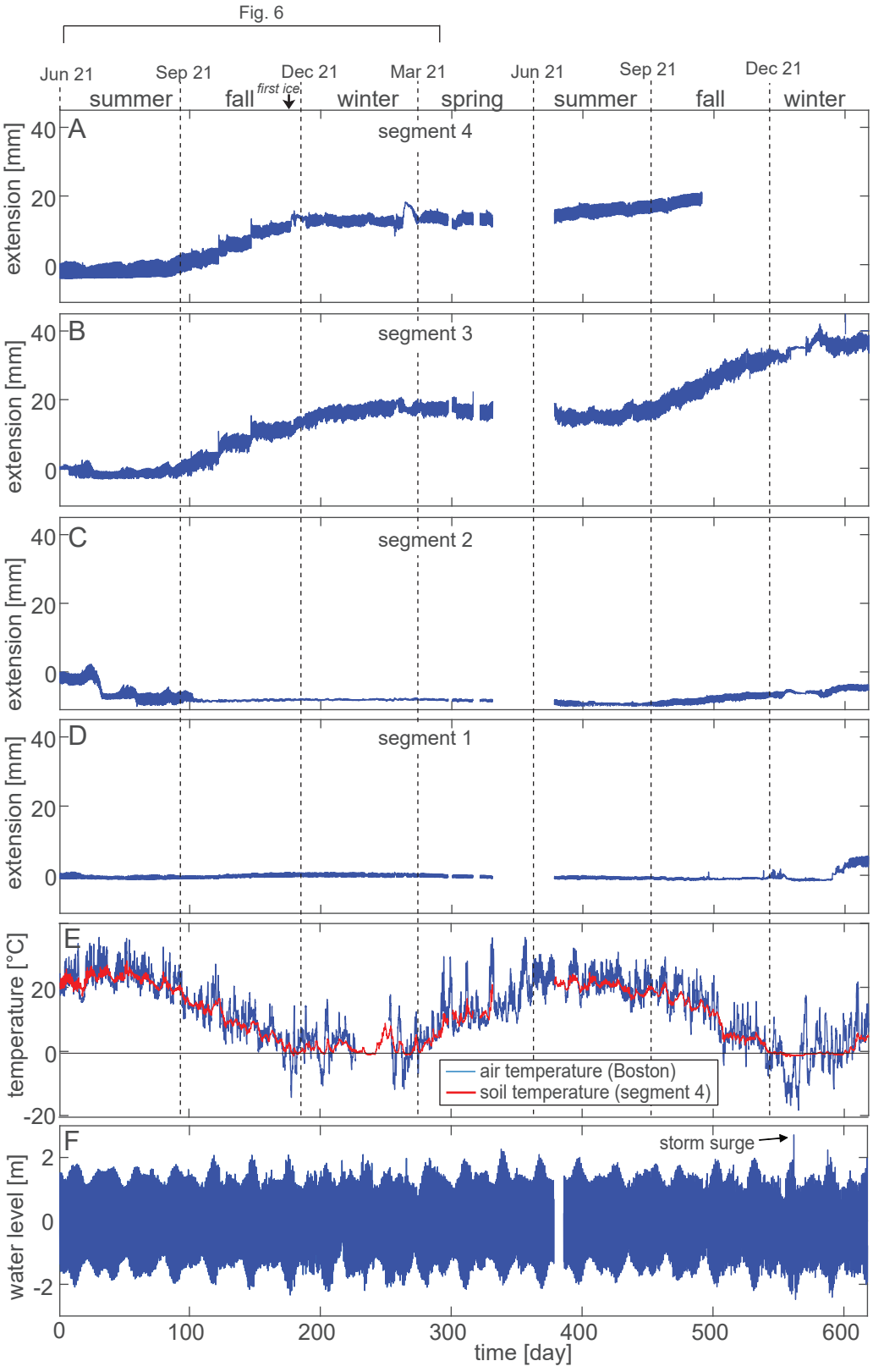
Fig. 6
Jun 21
Sep 21
Dec 21
Mar 21
Jun 21
Sep 21
Dec 21
summer
fall
first ice
winter
spring
summer
fall
winter
A
segment 4
B
segment 3
C
segment 2
D
segment 1
extension [mm]
40
20
0
E
temperature [°C]
20
0
-20
air temperature (Boston)
soil temperature (segment 4)
F
storm surge
water level [m]
2
0
-2
0
100
200
300
400
500
600
time [day]

Figure 3

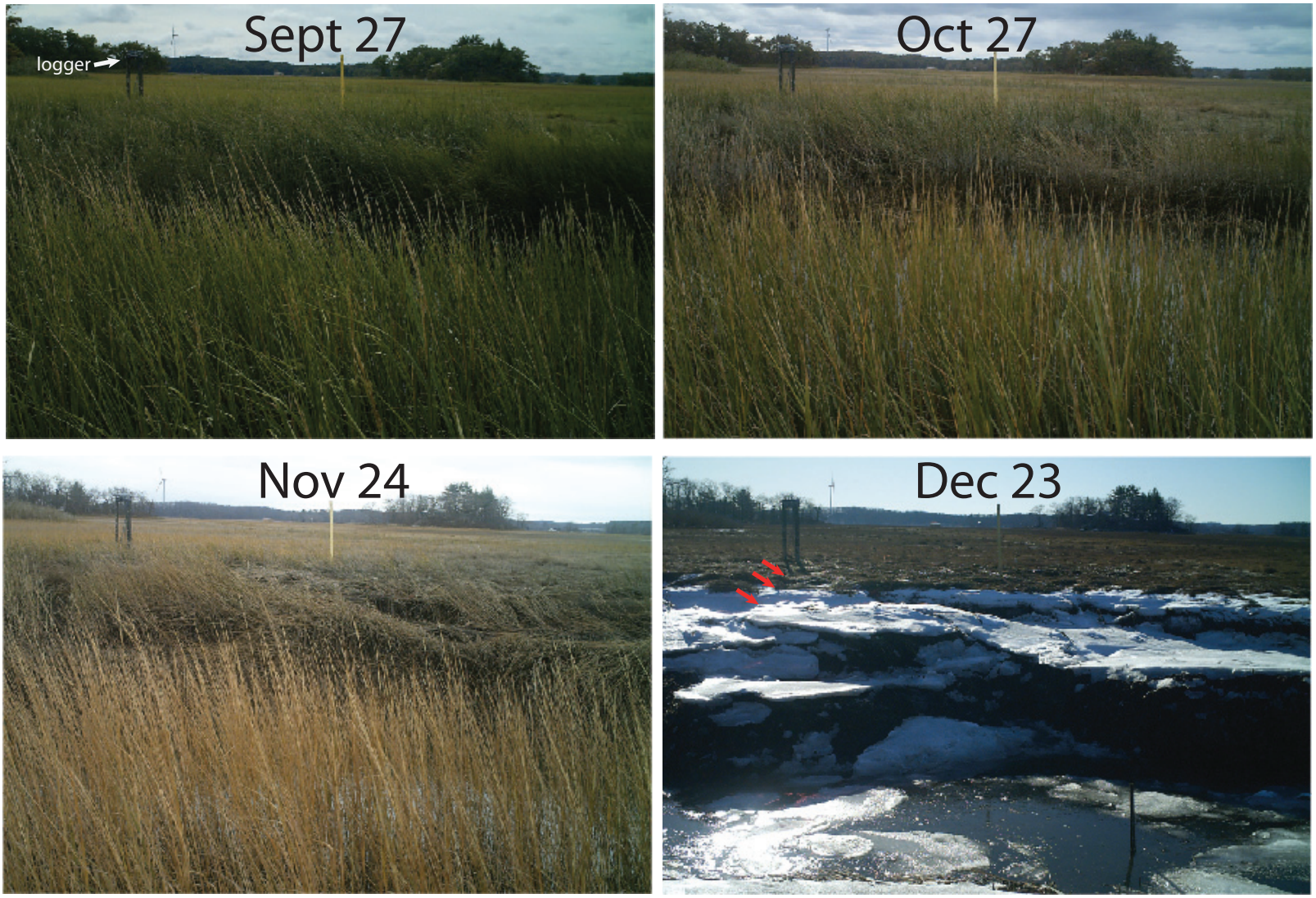

Figure 4

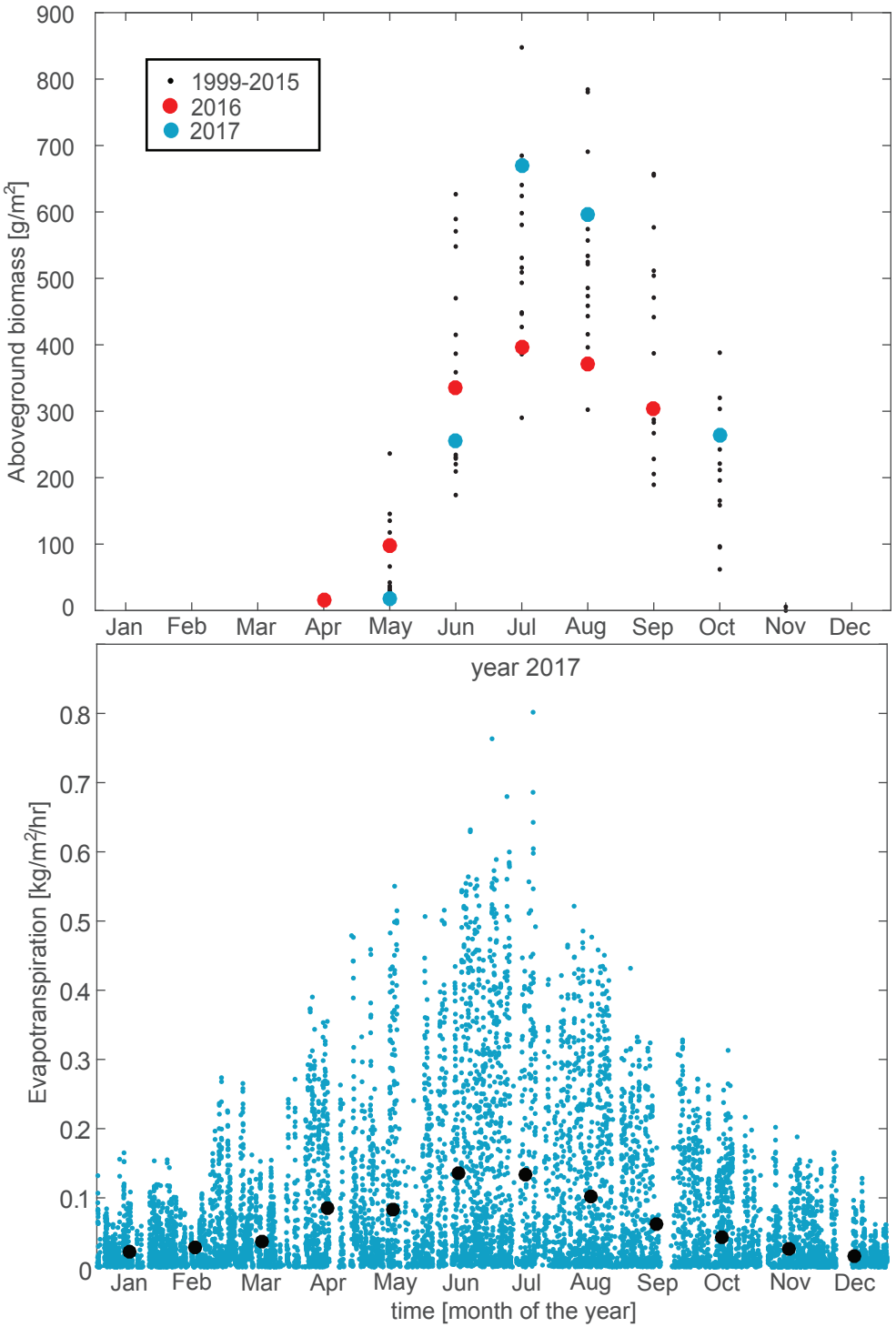
1999-2015
2016
2017
Aboveground biomass [g/m2]
0
100
200
300
400
500
600
700
800
900
Jan
Feb
Mar
Apr
May
Jun
Jul
Aug
Sep
Oct
Nov
Dec
year 2017
Evapotranspiration [kg/m2/hr]
0
0.1
0.2
0.3
0.4
0.5
0.6
0.7
0.8
time [month of the year]

Figure 5

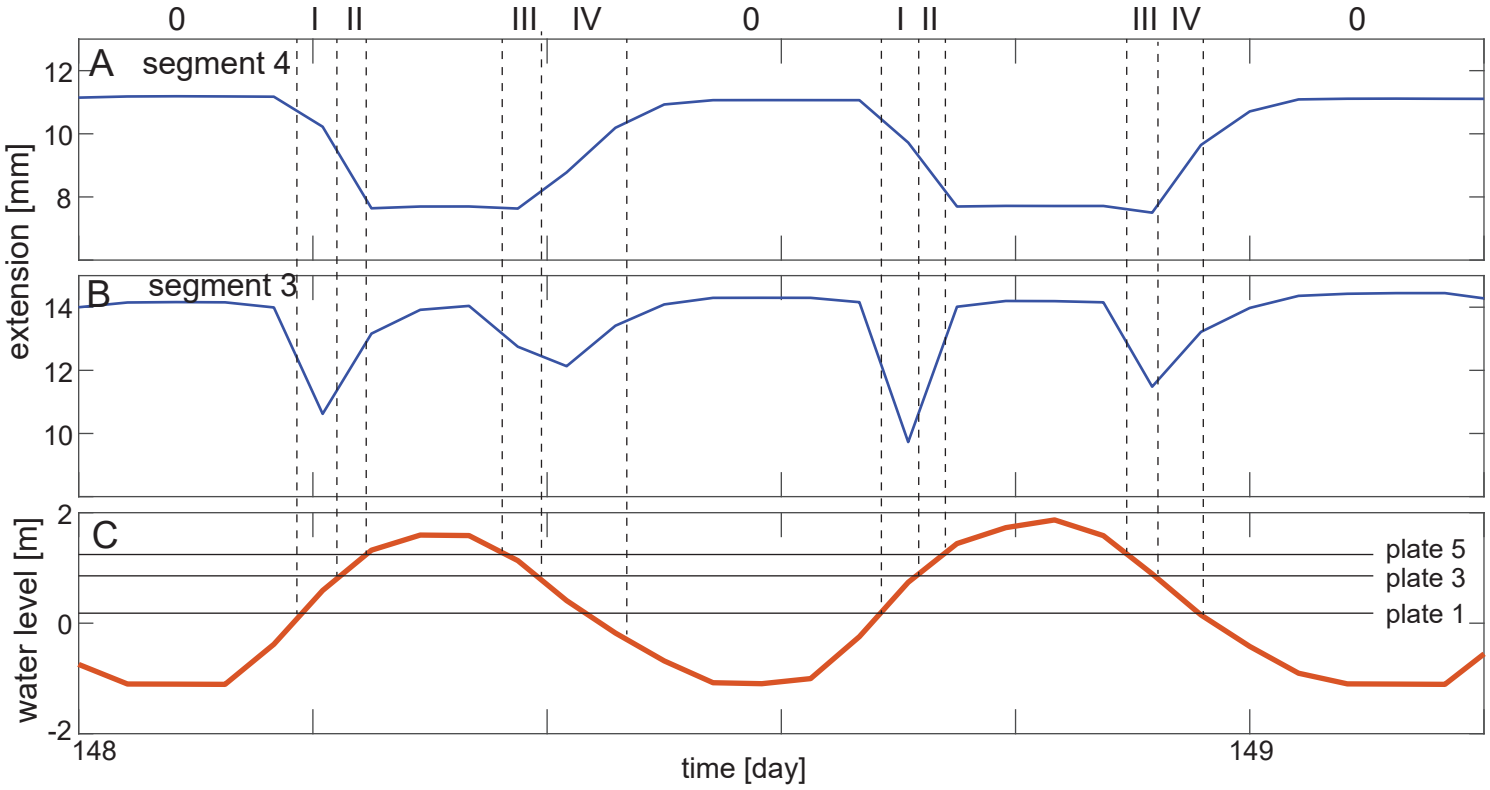
0
I
II
III
IV
0
I
II
III
IV
0
A
segment 4
B
segment 3
C
extension [mm]
water level [m]
plate 5
plate 3
plate 1
148
149
time [day]

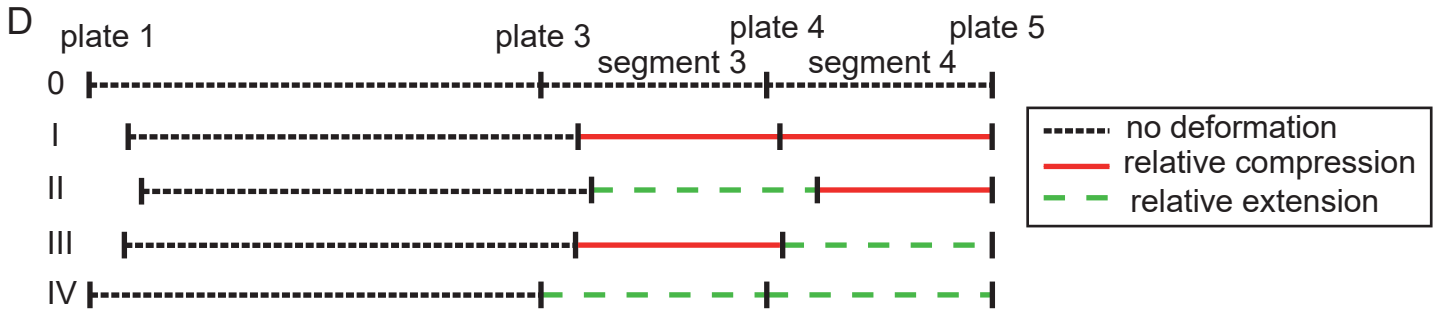
D
plate 1
plate 3
plate 4
plate 5
segment 3
segment 4
0
I
II
III
IV
no deformation
relative compression
relative extension

Figure 6

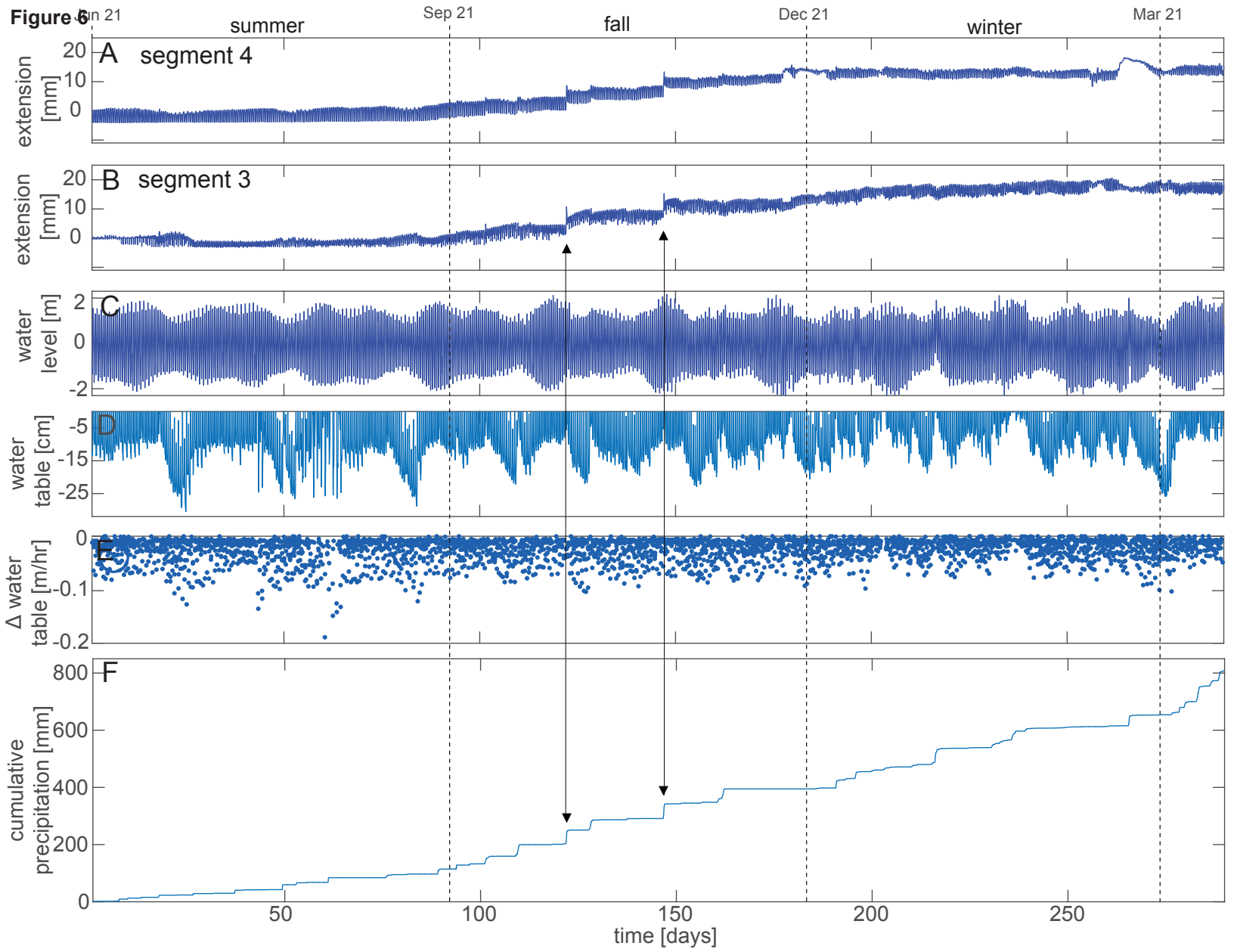
Jun 21
Sep 21
Dec 21
Mar 21
summer
fall
winter
A segment 4
extension [mm]
B segment 3
extension [mm]
C
water level [m]
D
water table [cm]
E
Δ water table [m/hr]
F
cumulative precipitation [mm]
time [days]

Figure 7

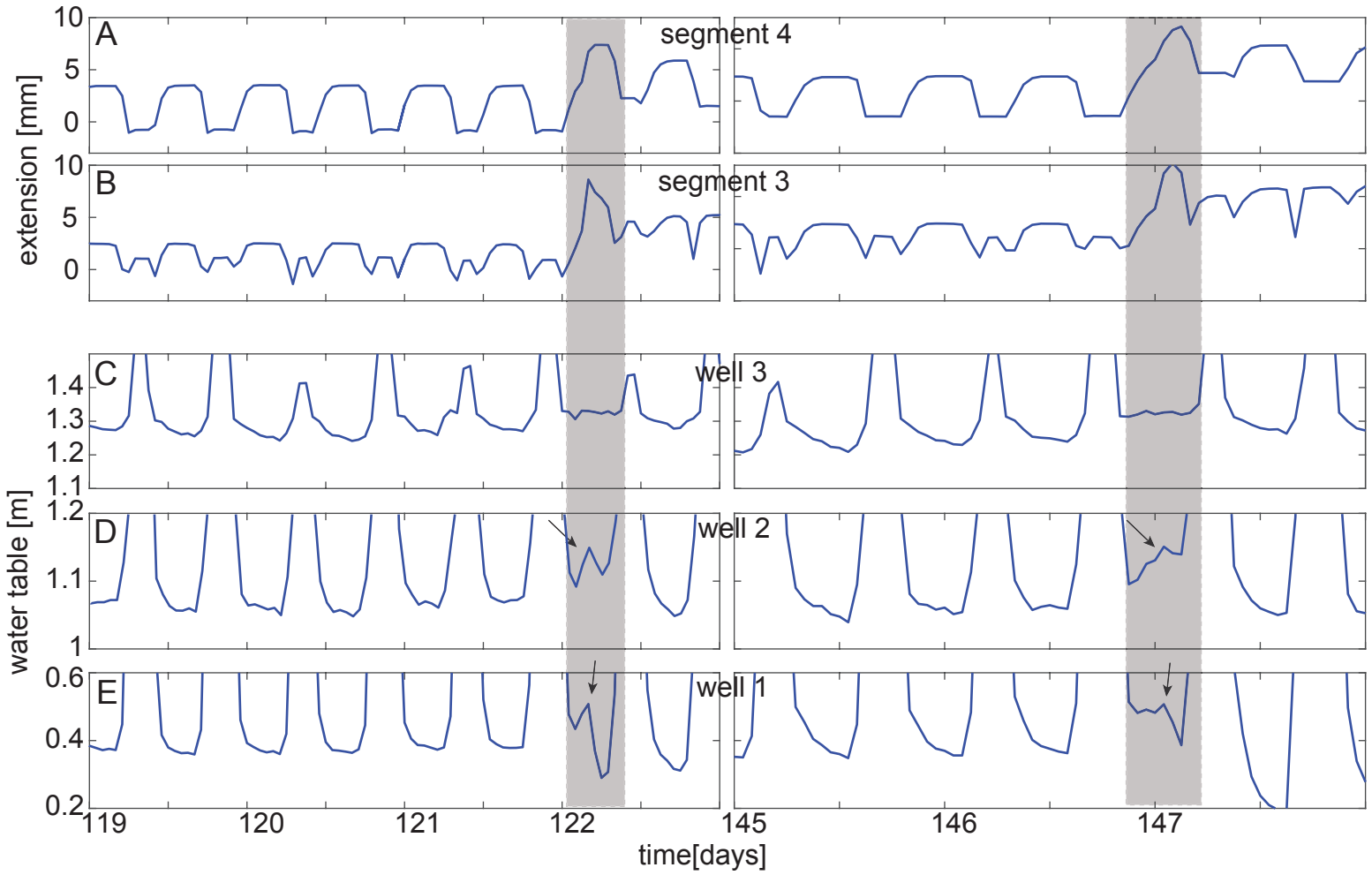
A
segment 4
B
segment 3
C
well 3
D
well 2
E
well 1
extension [mm]
water table [m]
time[days]
10
5
0
1.4
1.3
1.2
1.1
1
0.6
0.4
0.2
119
120
121
122
145
146
147

Figure 8

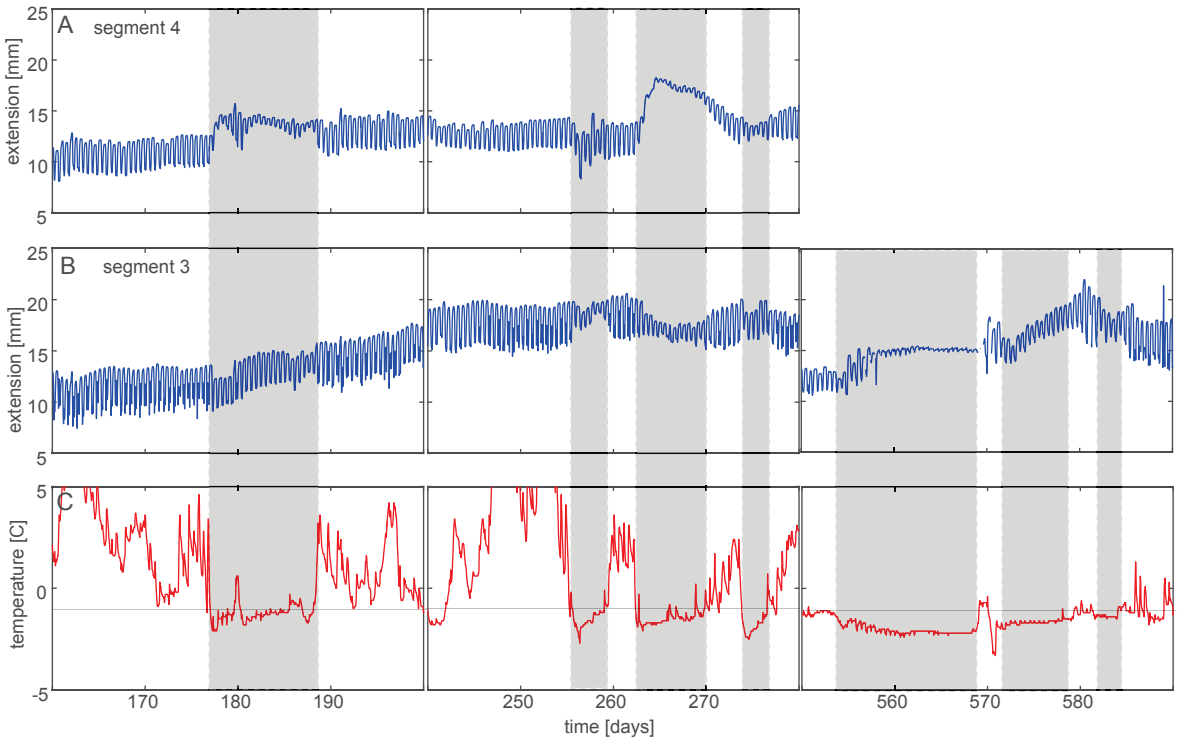
A
segment 4
extension [mm]
25
20
15
10
5
B
segment 3
extension [mm]
25
20
15
10
5
C
temperature [C]
5
0
-5
170
180
190
250
260
270
560
570
580
time [days]